IOP Conf. Series: Earth and Environmental Science **35** (2016) 012006 doi:10.1088/1755-1315/35/1/012006

DNS and measurements of scalar transfer across an air-water interface during inception and growth of Langmuir circulation

A Hafsi[1], Y Ma[2], M Buckley[2], A E Tejada-Martinez[1] and F Veron[2]

[1]Civil and Environmental Engineering Department, University of South Florida, 4202 E. Fowler Avenue, Tampa, FL 33620-535, USA
[2]School of Marine Science and Policy, College of Earth, Ocean and Environment, University of Delaware, Newark, DE 19716, USA

Email: aetejada@usf.edu and fveron@udel.edu

Abstract. Direct numerical simulations (DNS) of an initially quiescent coupled air-water interface driven by an air flow with free stream speed of 5 m/s have been conducted and scalar transfer from the air side to the water side and subsequent vertical transport in the water column have been analysed. Two simulations are compared: one with a freely deforming interface, giving rise to gravity-capillary waves and aqueous Langmuir turbulence (LT) characterized by small-scale (centimeter-scale) Langmuir cells (LC), and the other with the interface intentionally held flat, i.e., without LC. It is concluded that LT serves to enhance vertical transport of the scalar in the water side and in the process increases scalar transfer efficiency from the air side to the water side relative to the shear-dominated turbulence in the flat interface case. Furthermore, transition to LT was observed to be accompanied by a spike in scalar flux characterized by an order of magnitude increase. These episodic flux increases, if linked to gusts and overall unsteadiness in the wind field, are expected to be an important contributor in determining the long-term average of the air-sea gas fluxes.

1. Introduction

Turbulence associated with small scale (centimeter-scale) eddies known as Langmuir cells (or LCs) (see sketch in figure 1) can have direct impact on gas uptake by oceans. During low wind speeds (1–2 m/s), wave-current interaction leads to the generation of Langmuir turbulence characterized by these small scale LCs. As seen in the sketch of figure 1 (left panel), LC consists of parallel counter-rotating vortices roughly aligned in the direction of the wind. It is well known that LCs result from the interaction between the Stokes drift velocity induced by surface waves and the wind-driven shear current. The panel on the right in figure 1 shows a surface temperature image (with red indicating warmer temperatures and blue colder temperatures) of a wind-driven air-water interface during the development of small-scale Langmuir cells in laboratory experiments [4]. The presence of the Langmuir cells is manifested through the pattern in surface temperature. For example, the blue temperature streaks coincide with the surface convergence (downwelling) zones of the Langmuir cells.

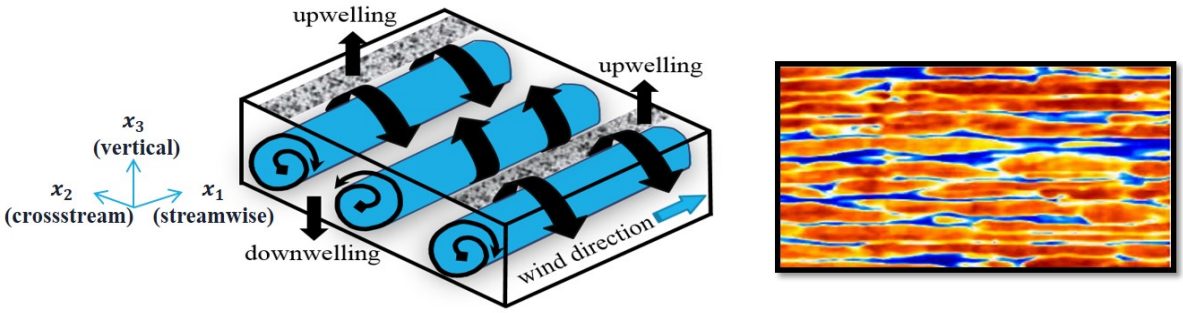

Figure 1. Sketch of LCs on left and surface manifestation of LCs on the air-water interface in terms of temperature on right (Veron and Melville [4]).

In the measurements of Veron and Melville [4] the inception of small-scale LCs and subsequent transition to Langmuir turbulence (prior to the onset of micro-breaking wind waves) lead to a 70% increase in gas transfer velocity (a measure of gas transfer efficiency), demonstrating the strong impact of LC on gas transfer across the air-water interface. Transition to Langmuir turbulence refers to when the initially coherent vortices become unstable and lose coherency as they start to interact with each other nonlinearly. The measurements of Veron and Melville [4] were collected under a gradually increasing wind with final speed of 5 m/s at a fetch of 10.72 m and during the presence of gravity-capillary waves possessing wavelengths up to 10–15 cm. More recent experiments made with sub-surface particle image velocimetry (PIV) and surface infrared radiometry were conducted in the large air-sea interaction facility at the University of Delaware. Several wind forcings were studied in order to obtain a variety of LC scales and intensities. It was found that the LCs provide intense surface renewal (see figure 2) and disrupt the near surface molecular layers. In particular, the LC rapidly transport surface layers to depth thereby transporting momentum away from the surface at rates much larger than that of molecular diffusion. The surface infrared measurements also provide air-water heat transfer velocity estimates. As a result strong correlations between scalar flux estimates and various kinematic quantities obtained from the PIV measurements and derived from moments of the sub-surface velocity gradient tensor were found. Figure 2 presents snapshots from a video filmed in these laboratory measurements taken at two different times, showing the progress of fluorescent dye initially deposited on the surface of a wind-driven air-water interface as a tracer during the presence of small-scale LCs. The images are in the crosswind-vertical plane, with the wind and waves traveling in the “into the page” direction. In figure 2 we can see the formation of pairs of vorticies that correspond to small-scale Langmuir cells. By comparing the progress of the fluorescent dye within the water side between an early time (figure 2a) and a later time (figure 2b) the effect of Langmuir cells on vertical transport of momentum and scalars can be observed.

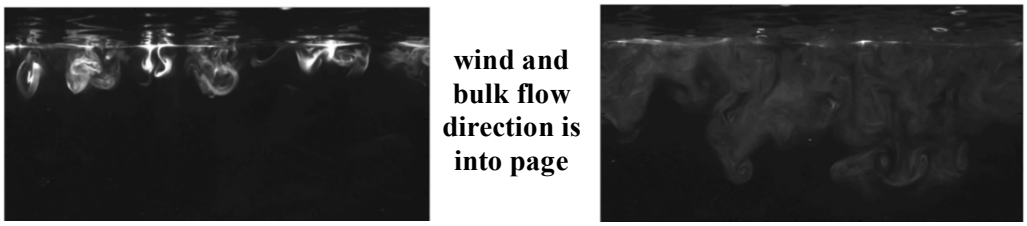

(a) (b)

Figure 2. (a) Fluorescent dye sprayed on a wind-driven air-water interface as a tracer during the presence of small-scale Langmuir cells at (a) an early time, (b) later time.

Komori *et al*. [3] performed a direct numerical simulation (DNS) similar to the laboratory setting of Veron and Melville [4]. In their DNS, LC-like structures coexisting with micro-breaking capillary waves riding on larger gravity-capillary waves were identified. However, a study of LC-like structures and their connection with gas transfer efficiency across the air-water interface was not explored. For the present study, a similar DNS of a wind-driven coupled air-water interface was conducted focusing on the vertical transport induced by small scale LCs to further establish the connection between the cells and scalar transfer across the interface.

2. DNS equations

The DNS equations consist of the incompressible continuity and the Navier–Stokes equations

$$\frac{\partial u_i}{\partial x_i} = 0 \tag{1}$$

$$\frac{\partial u_i}{\partial t} + u_j \frac{\partial u_i}{\partial x_j} = -\frac{1}{\rho}\frac{\partial p}{\partial x_i} + \nu \frac{\partial^2 u_i}{\partial x_j^2} \tag{2}$$

where u_i denotes the velocity field [$i = 1, 2$ and 3 represent the streamwise (or downwind), spanwise and vertical components, respectively], p is the pressure field, ν is the molecular kinematic viscosity and ρ is the density. In addition to the continuity and momentum (Navier–Stokes) equations to predict air and water flow velocities and pressures, the concentration of dissolved scalar (i.e., gas) in air and in water is predicted via an additional scalar transport equation:

$$\frac{\partial C}{\partial t} + u_j \frac{\partial C}{\partial x_j} = \kappa \frac{\partial^2 C}{\partial x_j^2} \tag{3}$$

where C is the concentration of the scalar and x is the molecular diffusivity of the scalar. In this study, as has been done in others, the ratio ν/κ or Schmidt number is set to 1 because this does not affect the fundamental turbulent mechanisms promoting scalar transfer across the interface.

The flow solver used in this research is based on the open source numerical collection of C++ libraries OpenFOAM (Open source Field Operations and Manipulations), which uses the finite volume method to discretize the continuity, Navier–Stokes and passive scalar equations. After the discretization of the Navier–Stokes equations, the resulting pressure-velocity coupling for the momentum equation is resolved using the pressure implicit with splitting of operators (PISO) method [2]. The diffusion terms are discretized using a central finite difference method whereas the nonlinear advection terms are discretized using a second order accurate upwind method. InterFOAM, a solver included with OpenFOAM, is used in order to track the air-water interface via a modified volume of fluid multiphase methodology.

3. Results and discussion

Simulations conducted follow closely the recent DNS of Komori *et al*. [3] of wind-driven, coupled air-water molecular boundary layers with a nonlinearly deformable surface (interface). The juxtaposed domains of the air and water fluids along an initially flat gas-liquid interface are represented by rectangular boxes with depths of δ and 2δ, respectively, where δ = 1.25 cm, while the streamwise and spanwise lengths are 8δ and 4δ, respectively (see figure 3a). A Cartesian coordinate system was adopted where the streamwise and spanwise directions are given by the x-axis and the y-axis, respectively, while the z-axis spans the air and water depths (see computational domain in figure 3a).

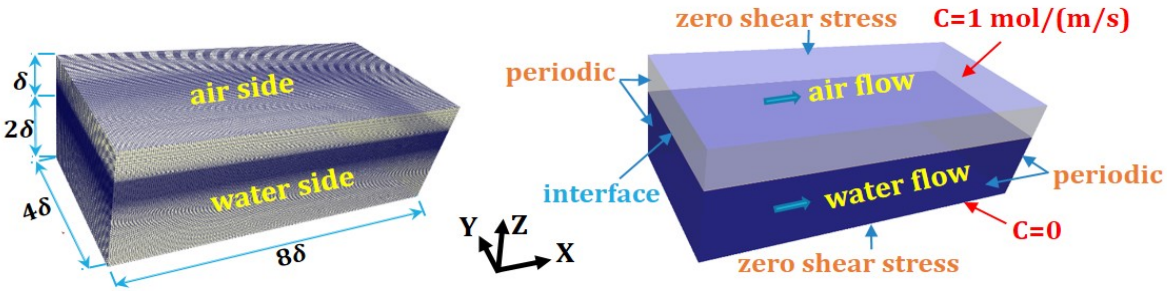

Figure 3. (a) Coupled air-water flow domain and computational mesh and (b) flow domain and boundary conditions: zero shear stress with zero normal flow and prescribed scalar concentration at top and bottom of the domain; periodicity in streamwise and spanwise directions.

The computational mesh shown in figure 3a consisted of 200 by 100 by 60 grid points on the air side and 200 by 100 by 120 grid points on the water side in the streamwise, spanwise and vertical directions, respectively. The computational mesh is uniform along the streamwise and spanwise directions, while a gradual mesh refining scheme was applied, in which the vertical mesh size becomes smaller in the approach to the air-water interface from either the water side or the air side (see figure 3). This meshing scheme was purposely used to resolve the air-water interface including centimeter-scale interfacial deformations as well as the molecular sub-layers in the air and water sides. The grid resolution for this mesh is between approximately 0.006 cm (near the air-water interface) and 0.05 cm (near the top and bottom of the domain).

Boundary conditions are summarized in figure 3b. The water side was started from rest with a flat air-water interface driven from above by the sudden imposition of a pre-computed, fully-developed boundary layer airflow driven by a pressure gradient (figure 4a). This boundary layer airflow was pre-computed (as a first step) in a separate simulation with a no-slip bottom and a zero-shear stress condition on top while maintaining periodic boundary conditions elsewhere (along streamwise and spanwise boundaries). The pre-computed airflow was characterized by far-field mean velocity $U_\infty = 5$ m/s, which is the same as the final far-field wind speed in the experiments of Veron and Melville [4]. For consistency, the computational mesh to run the preliminary airflow simulation was made identical to the air side portion of the air-water mesh in figure 3a.

The initial condition for scalar concentration was $C = 1$ mol/(m/s) in the air side and $C = 0$ in the water side. At the top of the domain (at the top of the air side) C was set to 1 mol/(m/s) and at the bottom of the domain (the bottom of the water side) C was set to 0, ensuring a flux of scalar from the air side to the water side (figure 3b).

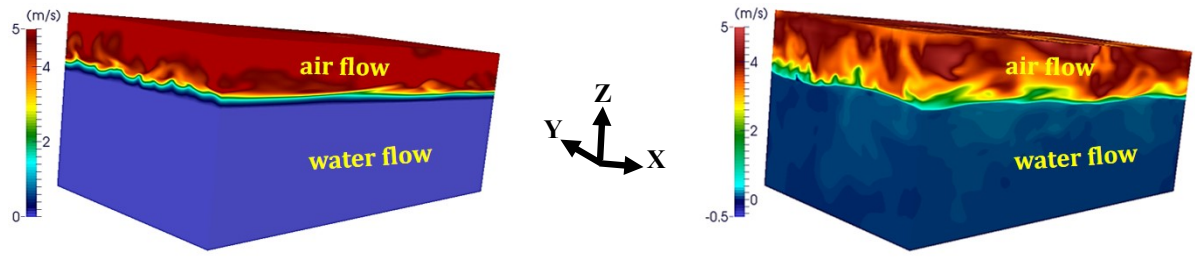

Figure 4. (a) Instantaneous snapshot of streamwise (x) velocity field distribution within the domain showing the turbulence in action within the air side and the water at rest as initial conditions. (b) Instantaneous snapshot of streamwise velocity field distribution within the domain showing turbulence in action within both the air and water sides after 5 s.

Figure 4b shows an instantaneous snapshot of streamwise (x) velocity field distribution within the domain showing the turbulence in action within both the air side and the water side at $t = 5$ s. Note the air flow velocities are much higher than the water flow velocities, as expected.

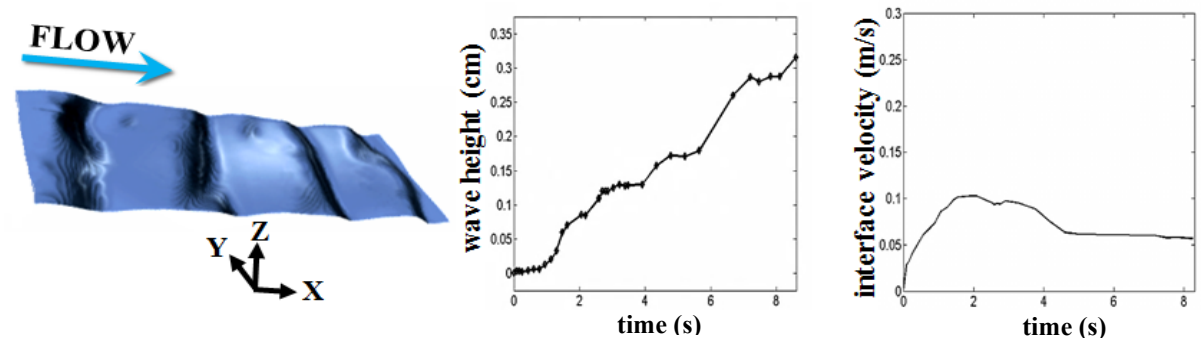

Figure 5. Left panel: the instantaneous air-water interface in DNS at $t = 2.5$ s. Middle panel: time series of the simulated maximum air-water interfacial wave heights. Right panel: time series of the simulated average streamwise velocity on the air-water interface.

Soon after the simulation started, at time $t = 1.5$ s, short capillary interfacial waves as small as 1 cm in wavelength and 0.25 mm in height were present accompanied by small capillary waves (ripples) with length scales of approximately 1–2 mm. The left panel in figure 5 shows a snapshot of the air-water interface deformation (corresponding to simulation time $t = 2.5$ s) of the DNS revealing gravity waves along with superimposed smaller capillary waves or ripples. The middle panel and right side panel of figure 5 show time series of maximum interfacial wave heights and average streamwise velocity on the interface, respectively. Trends observed in these records follow close to those observed in the DNS of Komori *et al*. [3].

As can be seen in figure 6a at $t = 0.5$ s, streamwise velocity fluctuations at the interface are characterized by smooth downwind elongated streaks. These narrow streaks are found to be parallel to each other, while alternating in sign in the spanwise direction. Starting at approximately $t = 1$ s (figure 6b), the streaky structure of the streamwise velocity fluctuation is disrupted by capillary wave deformations until about $t = 2.5$ s (figure 6c). This observed disruption is due to the fact that the downwind velocity fluctuation not only has a component due to the turbulence but it also has a significant capillary wave-induced component. As time progresses after $t = 2.5$ s, (e.g., at $t = 4$ s, figure 6d) the downwind elongated streaks re-emerge, due to the turbulent component of the velocity becoming more dominant than the wave-induced component. Re-emergence of downwind elongated streaks is indicative of the flow transitioning to Langmuir turbulence. Furthermore, the instantaneous scalar fluxes show a relative increase between $t = 2.5$ s (figure 6g) and $t = 4$ s (figure 6h). This increase is attributed to transition to Langmuir turbulence which contributes towards the enhancement of scalar uptake by the water. Note that the scalar flux is characterized by streaks similar to the velocity fluctuations.

Additionally, we compare results in terms of instantaneous streamwise vorticity in our simulation of the deforming air-water interface with instantaneous streamwise vorticity coming from a similar simulation but with the air-water interface held fixed (flat). The results from the flat interface case are shown on figures 7a and 7b and the results from the deforming interface case are shown on figures 7c and 7d. The deforming interface case is characterized by Langmuir cells growing in the cross-stream direction and in depth whereas the simulation with the flat interface shows smaller and less intense near-surface vortices.

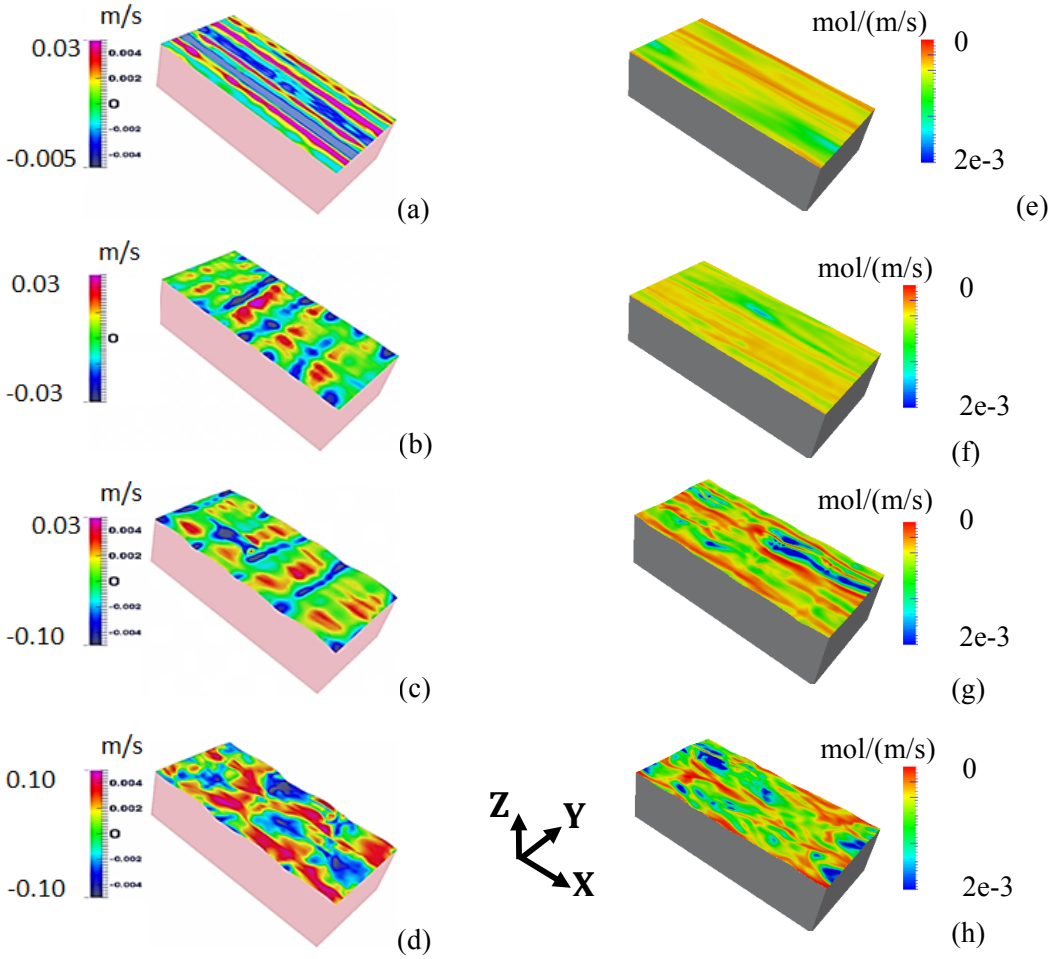

Figure 6. Instantaneous streamwise velocity fluctuation at (a) $t = 0.5$ s, (b) $t = 1$ s, (c) $t = 2.5$ s and (d) $t = 4$ s. Instantaneous scalar flux in mol/(m/s) at (e) $t = 0.5$ s and (f) $t = 1$ s, (g) $t = 2.5$ s and (h) $t = 4$ s.

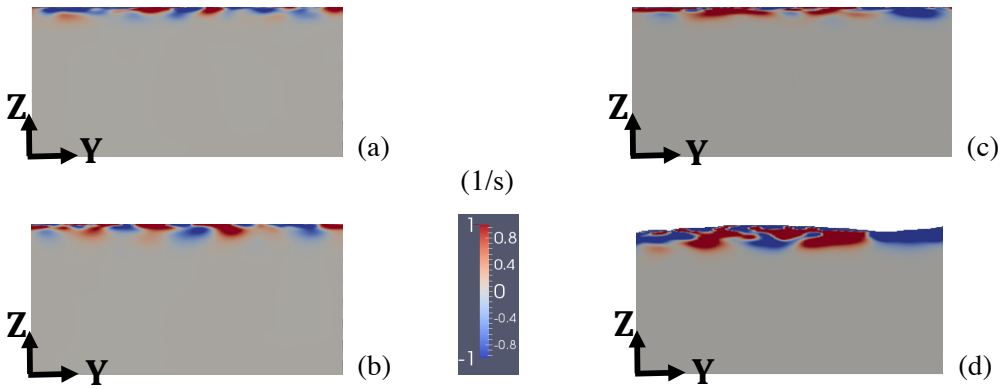

Figure 7. Instantaneous streamwise vorticity (1/s) from DNS with air-water interface held flat at (a) $t = 1$ s and (b) $t = 3$ s. Instantaneous streamwise vorticity (1/s) from DNS with freely deforming air-water interface at (c) $t = 1$s and (d) $t = 3$ s.

Moreover, prior to the transition to Langmuir turbulence, which was previously determined to be at approximately t = 2.5 s, both cases simulated (flat and deforming interface simulations) were compared in terms of depth profiles of mean scalar concentration in the water column. It was found that both cases possess similar concentration profiles through t = 2.5 s (not shown). However, for times greater than 2.5 s, the Langmuir turbulence and associated Langmuir cells in the deforming interface case generate greater vertical transport than the shear-generated turbulence in the flat interface case. From the depth profiles and instantaneous contours of scalar concentration shown in figure 8, we can conclude that the Langmuir turbulence penetrates deeper than the shear turbulence, thus the Langmuir turbulence is able to transport higher concentration fluid to greater depths. Note that as time progresses the difference between Langmuir turbulence penetration in the deforming interface case and the shear turbulence penetration in the flat interface case becomes more significant.

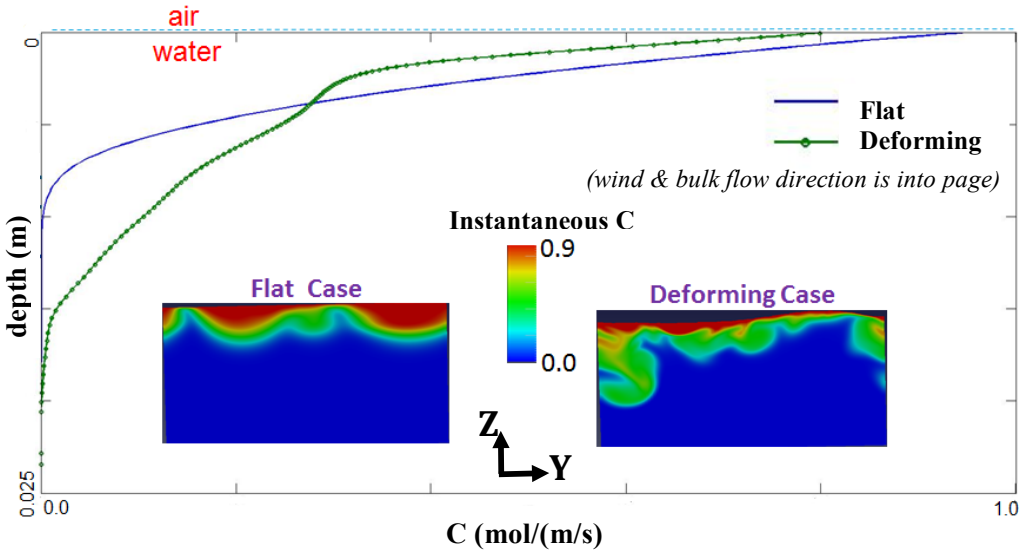

Figure 8. Depth profiles (averaged over streamwise and spanwise directions) and instantaneous snapshots of scalar concentration at time t = 4 s in the simulation with a deforming interface and the simulation with a flat interface.

The spatially averaged scalar flux across the wind-driven air-water interface for the flat and deforming interface cases are shown in figure 9. A dramatic explosion or spike of scalar flux is observed in the deforming case at approximately t = 2.5 s when the flow transitions to Langmuir turbulence. In contrast, a sudden increase in scalar flux is noticeably absent in the flat interface case. After this spike, the average scalar flux obtained in the deforming case decreases significantly but stabilizes at a mean value approximately two times greater than the scalar flux obtained in the flat case. In the field, it is likely that such gas flux spikes are correlated with wind transients or gusts and thus might be a dominant contributor to the long-term time-averaged gas flux.

Lastly, we calculate transfer velocity a measure of scalar transfer efficiency, following Kader *et al*. [1]:

$$k_L = \kappa \frac{\nabla C \cdot \boldsymbol{n}}{(C_i - C_{bulk})} \tag{4}$$

where C_i is streamwise and spanwise average concentration on the interface and C_{bulk} is bulk concentration calculated as

$$C_{bulk} = \int_0^{2\delta} \langle C \rangle_{x,y} \langle u \rangle_{x,y} dz \tag{5}$$

with $\langle \cdot \rangle_{x,y}$ denoting the average over streamwise and cross-stream directions. Due to the enhanced vertical transport induced by the Langmuir turbulence and associated cells, the bulk concentration is significantly greater in the interface deforming case compared to the flat interface case (figure 10). Ultimately this leads to a greater transfer velocity (k_L) in the deforming interface case (figure 11), as k_L is inversely proportional to the difference between concentration at the interface and bulk concentration (equation 4).

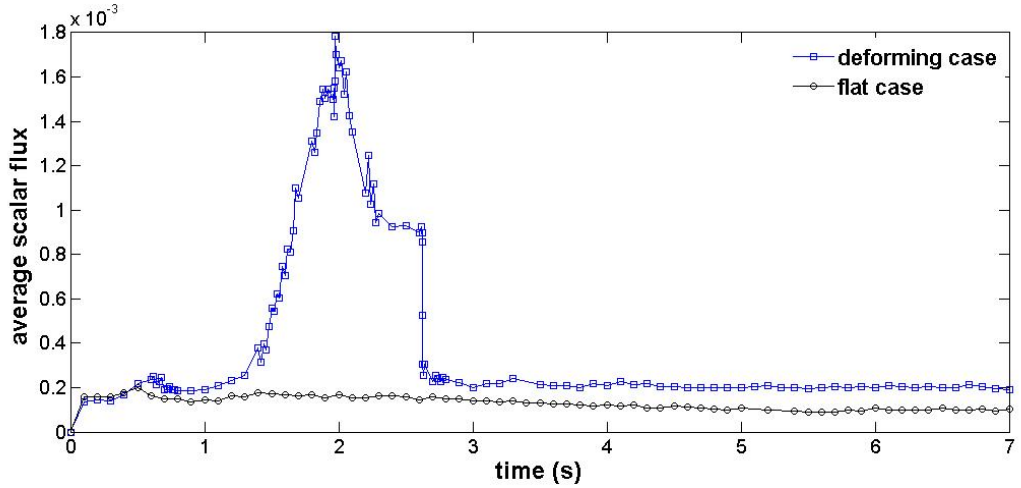

Figure 9. Average scalar flux through the air-water interface: $F = \kappa \nabla C \cdot \boldsymbol{n}$, where $\boldsymbol{n}$ is the unit normal to the interface.

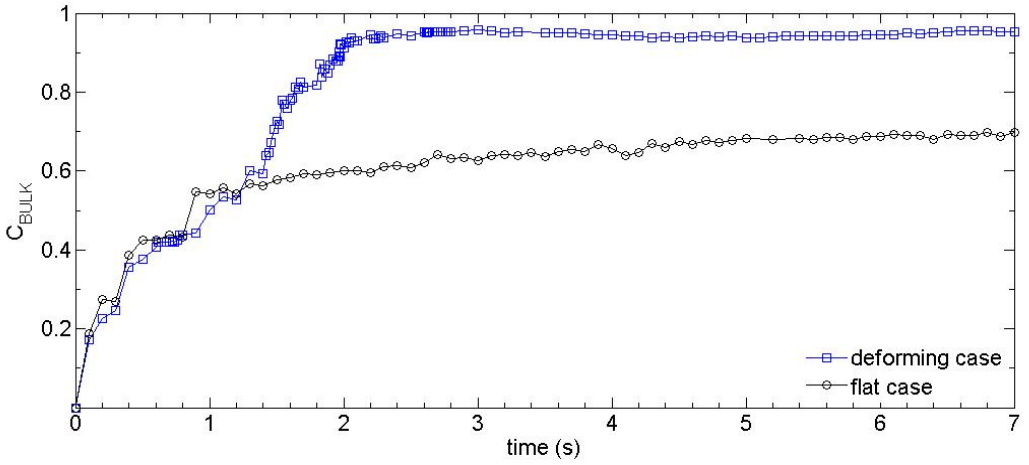

Figure 10. Bulk concentration of the air-water interface.

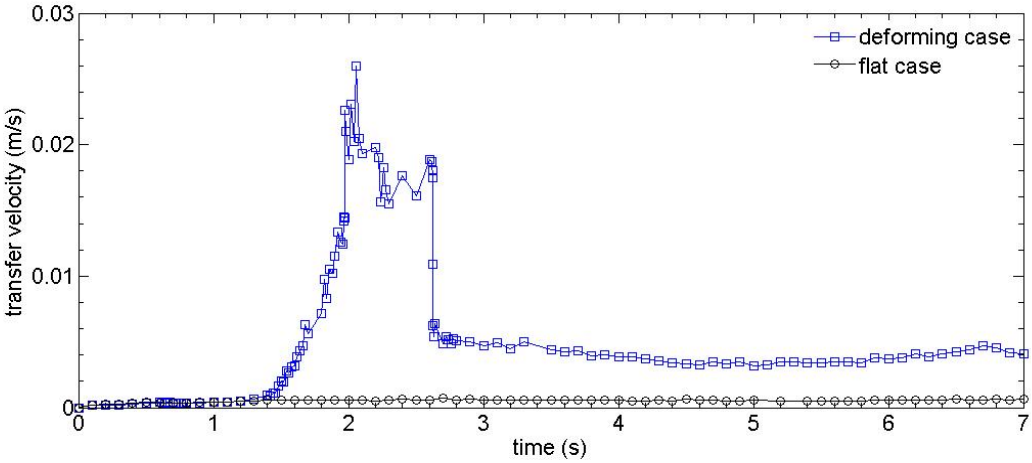

Figure 11. Transfer velocity.

4. Conclusion

The deforming interface and associated Langmuir turbulence play important roles in determining scalar flux across the interface and subsequent vertical transport of the scalar. Transition to Langmuir turbulence was observed to be accompanied by a spike in gas flux characterized by an order of magnitude increase. These episodic flux increases, if linked to gusts and unsteadiness in the wind field, are expected to be an important contributor in determining the long-term average of the air-sea fluxes. Finally, vertical transport induced by the Langmuir cells was seen to enhance bulk concentration throughout the water column which ultimately enhances transfer velocity. Future research will focus on understanding how the Langmuir turbulence affects scalar transfer at the interface via molecular diffusion.

References

[1] Kader B A and Yaglom A M 1972 *J. Heat Mass Transfer* **15** 2329
[2] Jasak H 1996 *Error Analysis and Estimation for the Finite Volume Method with Applications to Fluid Flows* (London: Imperial College)
[3] Komori S *et al* 2010 *J. Turbulence* **11** N32
[4] Veron F and Melville W K 2001 *J. Fluid. Mech.* **446** 25